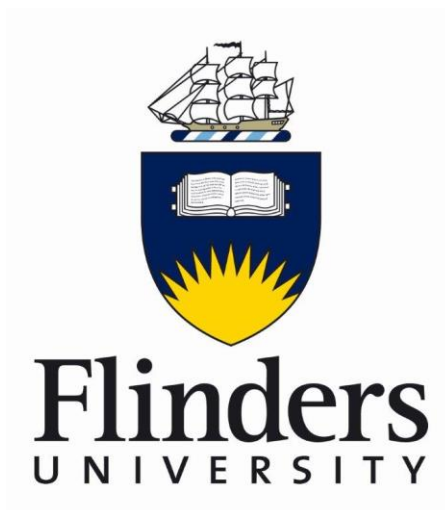


Electronic and Chemical Properties of Interfaces in Organic Photovoltaic Devices



*Thesis Presented to the School of Chemical & Physical Sciences, Faculty of Science
& Engineering of Flinders University in Candidacy for the Degree of*

Doctor of Philosophy

July 2014

Anirudh Sharma

Master of Nanotechnology

ॐ

श्रीश्री गुरु-गौराङ्गौ जयतः ।

कर्मण्येवाधिकारस्ते मा फलेषु कदाचन ।

मा कर्मफलहेतुर्भूर् मा ते संगोऽस्त्वकर्मणि ॥ ४७ ॥*

*Śrīmad Bhagavad Gītā, Chapter 2, Verse 47

“We are at the very beginning of time for the human race. It is not unreasonable that we grapple with problems. But there are tens of thousands of years in the future. Our responsibility is to do what we can, learn what we can, improve the solutions, and pass them on.”

- Richard P. Feynman

In Loving memory of my beloved chachu late

Mr. Anuj Sharma (1966- 1988)

*Dedicated to my grandparents late Mr. C. L. Sharma
(1923- 2004) and Mrs. C. V. Sharma (1930-2003)*

Table of Contents

Abstract	i
Declaration	iii
Acknowledgement	v
List of Publications	vii
Awards and Prizes	xi
List of Figures	xiii
List of Tables	xix
Abbreviations	xxi
Chapter 1: Introduction to Organic Solar Cells	1
1.1. Renewable Energy	1
1.2. Photovoltaic Technology	3
1.2.1. First Generation Solar Cells	4
1.2.2. Second Generation Solar Cells	4
1.2.3. Third Generation Solar Cells	5
1.3. Organic Photovoltaic Cells (OPVs)	6
1.3.1. Performance	6
1.3.2. Lifetime & Stability	8
1.3.3. Processing & Fabrication	8
1.4. Physics of Inorganic & Organic Photovoltaics	9
1.5. Device Structure & Principle of Operation	10
1.5.1. Single Layer OPVs	10
1.5.2. Bilayer Hetero-junction OPV's	11
1.5.3. Bulk Hetero-junction OPVs	12
1.5.4. Tandem OPVs	13
1.6. Materials in OPV's	14
1.6.1. Donor Materials	14

Table of Contents

1.6.2.	Acceptor Materials	14
1.6.3.	Transparent Electrode Materials	15
1.6.4.	Interface Materials	15
1.7.	Characterisation of OPVs	16
1.7.1.	Factors Influencing I_{sc} , V_{oc} , & FF	20
1.7.1.1.	Short Circuit Current	20
1.7.1.2.	Fill Factor	20
1.7.1.3.	Open Circuit Voltage	21
1.8.	Design of BHJ Devices	21
1.8.1.	Conventional Structures	21
1.8.2.	Inverted Structures	22
1.9.	References	25
Chapter 2: Electronic Properties of Interfaces		39
2.1.	Introduction	39
2.2.	Electronic Structure of Organic Semiconductor	39
2.3.	Metal-Organic Interfaces	40
2.3.1.	Interface Engineering	43
2.4.	Experimental Techniques Used in This Thesis	44
2.4.1.	Neutral Impact Collision Ion Scattering Spectroscopy (NICISS)	44
2.4.2.	X-ray & Ultraviolet Photoelectron Spectroscopy	46
2.4.3.	Atomic Force Microscopy (AFM) and Kelvin Probe Force Microscopy (KPFM)	51
2.5.	References	55
Chapter 3: Research Project		61
3.1.	Introduction	61
3.2.	ITO-PEDOT:PSS Interface In Conventional OPVs	61
3.3.	ZnO-Polymer Interface in Inverted OPVs	63
3.4.	Electronic Properties of Heterogeneous Surfaces	64
3.5.	References	66

Chapter 4: Role of Humidity on Indium and Tin Migration in Organic Photovoltaic Devices	69
4.1. Abstract	70
4.2. Introduction	71
4.3. Experimental	73
4.4. Results and Discussion	74
4.5. Conclusions	86
4.6. References	87
Chapter 5: Effect of Indium and Tin Contamination on the Efficiency and Electronic Properties of Organic Bulk Hetero-junction Solar Cells	91
5.1. Abstract	92
5.2. Introduction	93
5.3. Experimental	94
5.4. Results and Discussion	98
5.5. Conclusions	103
5.6. References	105
Chapter 6: Role of Zinc Oxide Thickness on the Photovoltaic Performance of Laminated Organic Bulk Hetero-junction Solar Cells	109
6.1. Abstract	110
6.2. Introduction	111
6.3. Experimental	112
6.4. Results and discussion	115
6.5. Conclusions	125
6.6. References	126
Chapter 7: Effect of Annealing Temperature of ZnO on the Energy Level Alignment in Inverted OPV's	129
7.1. Abstract	130
7.2. Introduction	131
7.3. Experimental	132

Table of Contents

7.4.	Results and discussion	134
7.5.	Conclusions	143
7.6.	References	145
Chapter 8: The Influence of ZnO Thickness and Stoichiometry on Device Performance of Inverted OPV's		149
8.1.	Abstract	150
8.2.	Introduction	151
8.3.	Experimental	152
8.4.	Results and Discussion	154
8.5.	Summary and Conclusions	160
8.6.	References	162
Chapter 9: Invisible High Workfunction Materials on Heterogenous Interfaces		165
9.1.	Abstract	166
9.2.	Introduction	167
9.3.	Results and Discussion	168
9.4.	Conclusions	175
9.5.	References	177
Chapter 10: Nanoscale Electronic Properties of ZnO Thin Films		179
10.1.	Abstract	180
10.2.	Introduction	181
10.3.	Experimental	182
10.4.	Results and Discussion	184
10.5.	Conclusions	189
10.6.	References	190
Chapter 11: Conclusions		193

Abstract

Organic Photovoltaics is a promising technology, which can potentially be a cheap source of clean and renewable energy in the near future. Despite tremendous research and development efforts in this field, organic solar cells still take a back stage in the mainstream photovoltaic market. Though the efficiencies have gradually increased to up to 12 %, device stability still remains a challenge limiting large-scale commercialization of this technology.

This dissertation is devoted primarily to the study of stability and performance-limiting electronic properties of device interfaces in both conventional and inverted OPVs. Given the importance of electrode workfunction in interfacial charge transport in devices, special focus was on better understanding the workfunction measurements on heterogeneous surfaces and precise measurement of lateral variations in workfunction on a nanoscale.

In particular, the interfacial instability of ITO-PEDOT:PSS interface in conventional OPVs was investigated and it was shown for the first time that the migration of indium and tin into the PEDOT:PSS was strongly driven by the presence of moisture and is not merely a diffusive process, as prior beliefs. It was systematically demonstrated that indium and tin contaminants can adversely affect the device performance by increasing the interfacial dipole at the ITO-PEDOT:PSS interface.

For inverted OPVs, a strong correlation between the processing conditions of ZnO and the device performance has been established. Changes in the electronic or structural properties of ZnO were demonstrated to be the driving force behind the strong dependence of device performance on the processing conditions of ZnO.

ZnO prepared via a range of techniques was studied and for all cases a minimum of 25 nm layer thickness was found to be essential to achieve optimum device performance. For sol-gel prepared ZnO, the workfunction was found to be independent of the layer thickness, whereas for ZnO layer casted from a colloidal solution, post annealing temperature was found to be critical and a minimum temperature of 200 °C was found to be essential in order to achieve desirable workfunction and electron affinity. As in case of pulsed laser deposited ZnO, stoichiometric ratio of Zn and O was also found to be dependent on the layer thickness and thicker layer (up to 100 nm) were found to get oxygen deficient with

Abstract

increasing thickness. A fully evolved band structure of ZnO was found to be absent for layers of thickness 12 nm or less, which explains the poor performance of such devices.

This work also establishes a clear understanding of workfunction measurements of heterogeneous surfaces with UPS. Surfaces with heterogeneity on a nanoscale were artificially created with a combination of energetically different materials. It was demonstrated that materials having relatively low workfunction have an enhanced secondary electron emission, which can be misleading in deriving absolute workfunction values from UPS measurements. This behaviour was found to be valid even for polycrystalline materials with nanoscale variations in workfunction such as ZnO. While nano-domains of different workfunctions across a nano-roughened ZnO surface were clearly demonstrated using KPFM, UPS results were found to be more representative of the domains corresponding to low workfunction regions.

Declaration

I certify that this thesis does not incorporate without acknowledgement any material previously submitted for a degree or diploma in any university; and that to the best of my knowledge and belief it does not contain any material previously published or written by another person except where due reference is made in the text.

Anirudh Sharma

Acknowledgement

The last four years have been an incredible phase of my life, which witnessed a transition of an inquisitive student to an independent scientist. My PhD journey was full of stirring experiences with fascinating science around me. As this enriching and unique PhD journey comes to an end, I would like to take this opportunity to acknowledge and thank all those who helped me either towards the completion of this dissertation or those who made my Australian odyssey, a memorable journey.

Firstly, I am deeply thankful to my advisor, Prof. David Lewis, for his invaluable guidance throughout my PhD journey and for his intellectual contribution, which helped me compile this work. I joined David's group as a Master's student and since then he has always been a constant source of support and inspiration for me. I sincerely appreciate him for showing confidence in me and giving me the right opportunities. I would like to equally thank my co-advisor Prof. Gunther Andersson for supporting me not only academically but also through the emotional ups and downs of a PhD life. His selfless time and support were sometimes all that kept me going, not to mention the sweet birthday cards on my desk which Gunther never forgot to surprise me with.

I owe my deepest gratitude to my co-advisor at Commonwealth Scientific and Industrial Research Organisation (CSIRO), Dr. Scott E. Watkins for his time and guidance during my various trips to CSIRO's fabrication facility at Clayton, Melbourne. I would also like to thank Dr Rüdiger Berger at Max Planck Institute for Polymer Research (MPIP) for his valuable supervision during my visiting study in Germany. I feel privileged to have got an opportunity to work and gain invaluable experience at MPIP, one of the world's most accomplished research institutes.

I am also indebted to Dr. Mihail Ionescu from Australian Nuclear Science and Technology Organisation (ANSTO) for helping me with Rutherford backscattering experiments and Dr. Joseph Franklin from Imperial College, London for his collaboration on PLD ZnO study. I must also acknowledge my colleagues at CSIRO, Dr Birendra Singh for his assistance with device fabrication, Dr. Jacek Jasieniak for providing ZnO particle ink and Dr. Gerry Wilson, for fruitful discussions.

I would like to extend my special thanks to Prof. Colin Raston for many stimulating

Acknowledgement

discussions and mentoring that has greatly benefited me in structuring this thesis in its current form. I would also like to show my gratitude to all my past and present colleagues in all the groups I have worked with, for their help and support especially Marie-Claire Hermant, Natalya Schmerl, Ben Chambers, Chris Ridings, Daniel Mangos, Daniel Gruszecki, Ashley Johns, Sean Clark, Sian La Vars at Flinders University and Dan Lee, Victor Bergmann, Anna Domanski, Dominic Pilat, Uwe Rietzler, Maria Untch and Prince Ravat at MPIP.

I gratefully acknowledge the funding sources, which made my PhD work possible. I was awarded a research scholarship from Flinders University for three and half years of my PhD candidature and a full fee waiver during my PhD candidature from the Faculty of Science and Engineering. I am thankful to the CSIRO Future Manufacturing Flagship for awarding me with a PhD top-up research scholarship, Australian Nanotechnology Network (ANN) for a travel grant towards an international conference and a visiting scholarship from Max Planck Institute for Polymer Research, Mainz, towards my study trip to MPIP in 3rd year of my PhD. I would not have been able to attend over six international conferences and study trips without these fellowships.

I would like to thank my family for all their love and encouragement and especially my *Mom* and *Dad* who raised me with a love of science and constantly supported me in various capacities throughout this long journey. Most of all, I really appreciate my loving girlfriend not only for her love and support but also for patiently bearing with me in those final and stressful days of my PhD. I love u!

Lastly, many thanks to the almighty for bestowing upon me his choicest blessing in form of such wonderful mentors, colleagues, parents, friends, family and all the right opportunities that came my way!

Anirudh Sharma

Flinders University

July 2014

List of Publications

Refereed Journal Articles

1. **Anirudh Sharma**, Rüdiger Berger, Gunther Andersson, David A. Lewis. Nanoscale heterogeneity and workfunction variations in ZnO thin films, *Submitted*.
2. **Anirudh Sharma**, Joseph B. Franklin, Birendra Singh, Gunther Andersson, David A. Lewis. Electronic and chemical properties of ZnO in inverted OPV's, *Submitted*.
3. **Anirudh Sharma**, Rüdiger Berger, Gunther Andersson, David A. Lewis. Invisible high workfunction materials on heterogeneous interfaces. *Applied Surface Science*, *Accepted*.
4. **Anirudh Sharma**, Scott Watkins, Gunther Andersson, David Lewis. Effect of annealing temperature of ZnO on the energy level alignment in inverted organic photovoltaics (OPVs). *Energy Technology*, 2014, 2 (5) pp. 462-468.
5. **Anirudh Sharma**, Mihail Ionescu, Gunther Andersson and David Lewis. Role of zinc oxide thickness on the photovoltaic performance of laminated organic bulk hetero-junction solar cells. *Solar Energy Materials and Solar Cells*, 2013, 115 pp. 64-70.
6. **Anirudh Sharma**, Scott Watkins, David Lewis and Gunther Andersson. Effect of indium and tin contamination on the efficiency and electronic properties of organic bulk hetero-junction solar cells. *Solar Energy Materials and Solar Cells*, 2011, 95(12) pp. 3251-3255.
7. **Anirudh Sharma**, Gunther Andersson and David Lewis. Role of humidity on indium and tin migration in organic photovoltaic devices. *Physical Chemistry Chemical Physics*, 2011, 13 pp. 4381-4387.

8. Lee Hoffman, Gunther Andersson, **Anirudh Sharma**, Stephen Clarke, and Nicolas Voelcker. New insights into the structure of PAMAM dendrimer/gold nanoparticle nanocomposites. *Langmuir*, 2011, 27(11) pp. 6759-6767.

Conference Proceedings

1. **Anirudh Sharma**, Gunther Andersson and David Lewis. Effect of ZnO layer thickness on the photovoltaic performance of laminated solar cells. *Nanomaterials for Green Technology*, Proceedings of the 3rd ISESCO International Workshop and Conference on Nanotechnology (IWCN 2012) Selangor, Malaysia. Dec 2012, pp. 57-57.
2. **Anirudh Sharma**, Scott E. Watkins, Gunther Andersson, and David Lewis. Instability of ITO-PEDOT:PSS interface in organic bulk hetero-junction solar cells and its effect on the efficiency and electronic properties of the device. *Thin Films and Nanomaterials* (Macmillan Advanced Research Series, India) edited by S. Jayakumar, M.D. Kannan, R. Balasundaraprabhu, S. Prasanna, Proceedings of the International Conference on Advanced Materials (ICAM 2011) Coimbatore, India. Dec 2011, pp. 212-215.

Presentations and Seminars

1. [Oral] **Anirudh Sharma**, Rüdiger Berger, Gunther Andersson, David Lewis. Workfunction measurement of heterogeneous surfaces. *Flinders Centre for Nanoscale Science and Technology (FCNST) Annual Conference, June 18, 2014, Adelaide, Australia.*
2. [Oral] **Anirudh Sharma**, Rüdiger Berger, Gunther Andersson, David Lewis. Nanoscale surface electronic properties of zinc oxide. *International Conference on Nanoscience and Nanotechnology (ICONN 2014)*, February 2- 6, 2014, Adelaide, Australia.
3. [Invited Oral] **Anirudh Sharma**, Scott Watkins, Gunther Andersson and David Lewis. ZnO buffer layer for OPV's: Interfacial energetics and its influence on device performance. *International Workshop and School on Nanotechnology (NanoS-E3 2013)*, September 15-20, 2013, Airlie Beach, Australia.
4. [Seminar] **Anirudh Sharma**, Scott Watkins, Gunther Andersson and David Lewis. Role of interfacial layers on the performance of OPV's. *Physics at Interfaces Research Group, Max Planck Institute for Polymer Research*, June 3, 2013, Mainz, Germany.
5. [Poster] **Anirudh Sharma**, Gunther Andersson and David Lewis. Role of ZnO layer thickness on the photovoltaic performance of OPV's. *Hybrid and Organic Photovoltaics Conference (HOPV 2013)*, May 5-8, 2013, Sevilla, Spain.
6. [Oral] **Anirudh Sharma**, Gunther Andersson and David Lewis. Effect of ZnO layer thickness on the photovoltaic performance of laminated OPV's. *The 3rd ISESCO International Workshop and Conference on Nanotechnology (IWCN2012)*, December 5-7, 2013, Universiti Kebangsaan (UKM) Malaysia.
7. [Seminar] **Anirudh Sharma**, Scott Watkins, Gunther Andersson and David Lewis. Role of interfaces on the photovoltaic performance of organic bulk hetero-junction solar cells. *South Australian Physical Chemistry Symposium*, December 3, 2012, University of Adelaide, Australia.

8. [Poster Prize] **Anirudh Sharma**, Gunther Andersson and David Lewis. Understanding the morphological and electronic properties of zinc oxide buffer layers used in inverted organic photovoltaic cells. *International Organic Excitonic Solar Cell Conference (IOESC 2012)*, September 3-7, 2012, Coolum Beach, Australia.
9. [Poster Prize] **Anirudh Sharma**, Scott Watkins, Gunther Andersson and David Lewis. Air-processed organic bulk hetero-junction solar cells fabricated with hot press lamination: A step towards roll-to-roll processing. *Flinders Centre for Nanoscale Science and Technology (FCNST) Annual Conference*, June 13, 2012, Adelaide, Australia.
10. [Oral] Jonathan Campbell, **Anirudh Sharma**, David Lewis, Thermomechanical behaviour of conducting polymer blends. *33rd Australian Polymer School*, February 12-15, 2012, Hobart, Australia.
11. [Oral] **Anirudh Sharma**, Scott Watkins, David Lewis and Gunther Andersson. Instability of ITO-PEDOT:PSS interface in organic bulk hetero-junction solar cells and its effect on the efficiency and electronic properties of the device. *International Conference on Advanced Materials (ICAM) / Indo-Norwegian Workshop on Solar Energy Materials and Applications*, December 12-16, 2011, Coimbatore, India.
12. [Oral] **Anirudh Sharma**, Scott Watkins, Gunther Andersson and David Lewis. Degradation of OPV's due to interfacial instability and an alternative approach towards roll-to-roll device fabrication. *Flinders Centre for Nanoscale Science and Technology (FCNST) Annual Conference*, July 18, 2011, Adelaide, Australia.
13. [Poster] **Anirudh Sharma**, Gunther Andersson and David Lewis. Stability of ITO-PEDOT:PSS interface in bulk hetero-junction solar cells. *Australian Research Network for Advanced Materials & Australian Research Council Nanotechnology Network Joint Annual Workshop (ARNAM/ARCNN 2010)*, July 19-23, 2010, Adelaide, Australia.

Awards and Prizes

2014: **Best Presentation Award**

Flinders Centre for Nanoscale Science and Technology (FCNST) Annual Conference, Australia.

2013: **Visiting Research Fellowship**

Max Planck Institute for Polymer Research (MPIP), Germany.

2012: **Conference Travel Grant**

Australian Nanotechnology Network (ANN), Australia.

2012: **Poster Prize**

International Organic Excitonic Solar Cell Conference (IOESC), Coolumb Beach, Australia.

2012: **University Finalist (2nd prize- Faculty of Sci. & Eng.)**

Flinders University 3MT Competition, Australia.

2012: **Poster Prize**

Flinders Centre for Nanoscale Science and Technology (FCNST) Annual Conference, Australia.

2011: **Chancellor's Letter of Commendation for Academic Excellence**

Flinders University, Australia.

2011: **Tuition Fee Waiver**

Faculty of Science & Engineering, Flinders University, Australia.

2010: **Postgraduate Research Top-up Scholarship**

*Future Manufacturing Flagship, Commonwealth Scientific and Industrial
Research Organization (CSIRO), Australia.*

2010: **Privately Funded Postgraduate Research Scholarship**

Flinders University, Australia.

2009: **Summer Research Scholarship**

Faculty of Science & Engineering, Flinders University, Australia.

List of Figures

Figure 1.1: Comparison of renewable and finite energy reserves (Terawatt-years). Yearly potential is shown for the renewable resources and total recoverable reserves are shown for the finite resources. Taken from Perez et al. ^[5]	02
Figure 1.2: Global production of photovoltaic cells and modules from 2000 to 2012. Taken from PV status report, 2012. ^[7]	03
Figure 1.3: Cumulative installation of photovoltaic cells and modules from 200 to 2012. Taken from PV status report, 2012. ^[7]	03
Figure 1.4: Cost and efficiency projections for 1 st , 2 nd and 3 rd generation solar cells. Taken from reference [18].	05
Figure 1.5: Record efficiencies reported for OPVs in the last three decades. Taken from reference [33].	07
Figure 1.6: Venn diagram depicting a favourable scenario for successful commercialization of OPVs where the efficiency, stability and processing is optimally achieved. Adapted from reference [35].	07
Figure 1.7: A schematic depiction of the light harvesting process in an OPV. ϕ_{ITO} and ϕ_{Al} are the workfunctions of the ITO and aluminium electrode, respectively.	10
Figure 1.8: Schematic representation of (a) structure of a single layer OPV (b) a Schottky contact at the p-type polymer-Al interface.	11
Figure 1.9: Schematic of a bilayer OPV with sequential deposition of donor and acceptor material and (on the right) exciton dissociation at the donor acceptor interface.	12
Figure 1.10: Schematic of a BHJ OPV with a blended donor and acceptor organic layer.	13
Figure 1.11: Schematic of a tandem OPV with two sub cells complimenting the absorption spectral window. Taken from Ameri et al. ^[96]	13
Figure 1.12: AM0 extra-terrestrial spectrum and American Society for Testing and Materials	

(ASTM) G159 (direct normal and global, 37° sun-facing tilted) terrestrial spectra as tabulated in the current standard. Taken from Gueymard et al.^[139]17

Figure 1.13: Equivalent circuit of a solar cell.17

Figure 1.14: I-V curve of a solar cell under illumination and in dark. The figure relates the I-V characteristics of a device qualitatively to the energy level diagrams. The broken line connecting the I_{sc} and V_{oc} corresponds to the shape of an ideal device (100 % FF).19

Figure 1.15: Schematic showing the distribution of the square of the optical field strength across various material layers in a conventional OPV with and without an optical spacer. Taken from Steim et al.^[137]20

Figure 1.16: Schematic of a conventional and an inverted device structure.22

Figure 2.1: Electronic structure of (a) an organic solid (b) simplified version of its energy levels. Taken from Ishii et al.^[8]40

Figure 2.2: Electronic structure of a metal-organic interface depicting a scenario with vacuum level alignment between the two materials. Taken from Seki et. al.^[10]41

Figure 2.3: Schematic depiction of a metal-organic interface in electrical equilibrium (Fermi levels aligned) with the band bending assuming (a) common VL (b) interface dipole formation between the metal and organic layer resulting in VL shift. ϕ_B^n and ϕ_B^p are the electron and hole injection barriers, respectively and the organic layer is charged positive, thus making the Δ negative. Taken from Ishii et al.^[8]41

Figure 2.4: Schematic depicting charge transfer induced dipole formation resulting in (a) downshift or (b) upshift of the vacuum level by electronic charge transfer to or from the substrate, respectively. Taken from Braun et al.^[5]42

Figure 2.5: A schematic depicting the basic setup of NICISS instrument. Projectiles backscattered at about 168° from normal are detected with the TOF detector.45

Figure 2.6: A schematic depicting the working principle of a photoemission spectrometer. Monochromatic photons with certain energy $h\nu$ are incident at certain angle Ψ on the sample surface. Adapted from Reinert et al.^[43a]47

Figure 2.7: UP spectrum of a clean Au surface. Adapted from Helander et al. ^[45]	49
Figure 2.8: Schematic of UP spectra depicting photoemission from a metal, an organic layer and the corresponding shift in the vacuum level and at the Fermi edge. Taken from Ishii et al. ^[8]	51
Figure 2.9: Basic schematic of an AFM. Taken from Butt et al. ^[52]	52
Figure 2.10: Energy level alignment of the AFM tip and sample when (a) tip and sample are at a distance ‘d’ (b) when tip and sample are electrically in contact (c) when an external bias equal to the V_{CPD} is applied between the tip and the sample. Taken from Melitz et al. ^[53]	53
Figure 3.1: Schematic of a conventional OPV depicting indium and tin migration across the ITO-PEDOT:PSS interface.	62
Figure 4.1: NICIS spectra of PEDOT:PSS spin-coated on (a) silicon substrate (b) ITO and exposed to 56 % RH for 48 hours. To the spectrum of PEDOT:PSS on ITO, an offset is added for clarity.	75
Figure 4.2: Concentration depth profiles of (a) indium/tin and sulphur (b) oxygen and carbon (c) indium/tin migrated into the PEDOT:PSS thin film. The PEDOT:PSS film was spin-coated on ITO and exposed to 56 % RH for 48 hours.	77
Figure 4.3: Time dependence of indium/tin migration into thin PEDOT:PSS films. The concentration shown is the bulk concentration in the PEDOT:PSS film. In (a) the concentration of films stored under vacuum are shown, in (b) of samples exposed to 56 % RH. In (c) the bulk concentration of samples exposed to various RH are compared.	80
Figure 4.4: Time dependence of the indium/tin migration into PEDOT:PSS thin films after the films have been dried for 24 hours in vacuum.	81
Figure 4.5: XP spectra of (a) indium at the surface of pristine ITO and (b) indium found in a PEDOT:PSS film spin-coated on ITO and exposed to 56 % RH. The pristine ITO has a large peak at 444.7 eV and a small peak at 446.0 eV. In the spectrum of the PEDOT:PSS film the peak at 444.7 eV has disappeared and only a peak at 446.3 eV is found. In (c) XP spectra of tin of pristine ITO (broken line spectrum) and of tin in the PEDOT:PSS (bold line spectrum) is shown. The count rate of the tin spectra is much lower due to the lower concentration in ITO compared to indium. Thus no fits to the spectra are shown. However, a shift in the peak	

position of tin can clearly be identified.	84
Figure 5.1: Schematic representation of the fabricated device structure.	95
Figure 5.2: J-V characteristics of device A, B and C.	99
Figure 5.3: UP spectra of the PEDOT:PSS films spin-coated on ITO substrates. The secondary electron cut-off of sample B and sample C is shifted for 0.31 eV relative to that of sample A.	100
Figure 5.4: Low binding energy side of the UP spectra obtained from samples A, B and C.	102
Figure 6.1: Schematic of an inverted device fabricated using lamination technique.	111
Figure 6.2: 3-dimensional images of AFM scans (2x2 micron) showing the morphology of (X) cleaned ITO (a) sample A (b) sample B (c) sample C (d) sample C on a 1x1 micron scale.	116
Figure 6.3: RB spectra of ZnO thin film acquired from sample A.	117
Figure 6.4: Mass loss observed on conversion of zinc acetate to zinc oxide using ethanol as the precursor solvent. Inset shows a full-scale image of the same.	118
Figure 6.5: Mass loss observed on conversion of zinc acetate to zinc oxide with an isothermal hold at 300 °C.	119
Figure 6.6: High resolution spectra of Zn 2p and O1s recorded from sample C.	120
Figure 6.7: UP spectra of ZnO layers in sample A, B and C. The inset picture shows a closer look at the secondary electron cut-off.	121
Figure 6.8: J-V characteristics of laminated devices with zinc oxide buffer layers of different thickness and morphologies. Device X: without zinc oxide buffer layer, device A, B and C were fabricated using ZnO buffer layers similar to samples A, B and C, as summarised in Table 6.1.	122
Figure 6.9: Variation of series and shunt resistance with increase in the ZnO thickness. A, B and C corresponds to the resistance values of device A, B and C respectively.	124
Figure 7.1: Schematic of an inverted OPV incorporating ZnO particle layer.	131

Figure 7.2: J-V characteristics of best devices fabricated with ZnO particle layer annealed at various temperatures.	135
Figure 7.3: UP spectra of ZnO nanoparticle layers annealed at various temperatures.	137
Figure 7.4: Energy level alignment of ZnO nanoparticle layer with the acceptor (PCBM) in the BHJ in inverted OPV. Energy offset between the ZnO-PCBM interface is showed in red (in case of 150 °C annealing) and green (in case of 250 °C annealing). The value for the dipole used to construct the energy diagram is based on an assumption. The implications of this assumption are discussed in the main body of the work.	138
Figure 7.5: Core level XPS of Zn 2p 3/2.	139
Figure 7.6: Core level XPS of O 1s.	140
Figure 7.7: UP spectra from samples A, B, C and D depicting the three characteristic peak emissions.	141
Figure 7.8: Core level XPS of C 1s.	142
Figure 8.1: J-V characteristics of devices fabricated using ZnO buffer layer of different thicknesses.	154
Figure 8.2: Surface morphology (2 x 2 μm scans) of ITO and ZnO modified ITO substrates with various thicknesses of ZnO.	155
Figure 8.3: Normalised (a) secondary electron cut-off (b) valence band region of the UP spectra of ZnO modified ITO substrates.	157
Figure 8.4: Core level XP spectra of Zn 2p _{3/2} (left) and O 1s (right).	158
Figure 8.5: Normalised VBXP spectra of ZnO coated ITO substrates.	159
Figure 8.6: Plot depicting the O:Zn ratios (measured from XPS and VBXPS) plotted against the ZnO film thickness. The ratios calculated from VBXPS are only a quantitative estimation from the Zn 3d and O 2p peak heights from VBXP spectra and do not represent the atomic ratios of Zn and O in ZnO.	160
Figure 9.1: A schematic depicting potential photoemission processes during a UPS experiment and the labels indicate their contributions to an experimental spectrum for an Au-ITO	

heterogeneous surface prepared using TEM grid of mesh size 300.	169
Figure 9.2: Optical image (on the left) of the grid pattern created on an ITO substrate by thermally evaporating Au using a TEM grid of mesh 300 as a mask. On the right side is a SEM image showing a blown out grid to scale.	170
Figure 9.3: The normalised secondary electron cut-off and the valence band region of the UP spectra acquired from samples for all three meshes. The determination of the height of the secondary electron cut-offs for ITO and Au is exemplified for the 100 mesh samples. The expanded region between 12 eV and 22 eV shows the Au 5d band used to determine Au coverage.	171
Figure 9.4: Plot showing the Au contribution in the secondary electron cut-off vs the intensity of the Au 5d signal.	172
Figure 9.5: Plot showing the FWHM of the Gaussian function as a function of pass energy.	175
Figure 10.1: UP spectra of the sol-gel prepared ZnO nanoparticle layer and nano-roughened ZnO layer (ridge structure). Inset shows the magnified version of the secondary electron cut-off depicting a second onset in the UP spectrum of the nano-roughened ZnO sample.	185
Figure 10.2 KPFM image showing the simultaneously acquired (a) topography (b) CPD of a cleaned ITO surface.	185
Figure 10.3 KPFM image showing the simultaneously acquired (a) topography (b) CPD of planar ZnO surface.	186
Figure 10.4 KPFM image showing the simultaneously acquired (a) topography (b) CPD of ZnO surface with nano-roughened morphology.	187
Figure 10.5: KPFM image (5 X 5 micron) showing (a) topography (b) CPD of the ITO-Ag patterned surface.	189

List of Tables

Table 4.1: Summary of various NCISS experiments performed to study the effect of different processing conditions on the migration process.	78
Table 4.2: Summary of bulk concentrations of indium/tin measured after different treatments.	82
Table 5.1: Summary of various exposure conditions used for different samples.	96
Table 6.1: Recipes for spin-coating various zinc oxide layers on ITO.	113
Table 6.2: Summary of the number of monolayer and thickness of ZnO buffer layer in various samples, assuming the X-ray density of ZnO layers.	118
Table 6.3: Workfunction values of ITO and ZnO layers with various thickness and morphologies.	121
Table 6.4: Summary of various device parameters obtained from different devices. Device X corresponds to device fabricated without a ZnO buffer layer. Device A, B and C corresponds to devices prepared using ZnO recipes of samples A, B and C.	123
Table 7.1: Average of various device parameters after annealing ZnO particle layer at different temperatures.	136
Table 7.2: XPS peak positions and atomic concentration of oxygen, carbon and zinc in various samples treated at different temperatures.	143
Table 8.1: Characteristics of PLD ZnO films with different thicknesses and the device performance parameters of inverted devices fabricated using the PLD ZnO as an electron transport layer.	156
Table 8.2: Oxygen to zinc ratio in ZnO films of various thicknesses, as measured from XPS.	160
Table 9.1: Amount of Au present on the sample surface and the corresponding positions of the secondary electron cut-offs.	174

Abbreviations

AFM	Atomic force microscope
ALD	Atomic layer deposition
AM	Air mass index
BHJ	Bulk hetero-junction
CPD	Contact potential difference
CSIRO	Commonwealth scientific and industrial research organization
DI	De-ionized
FWHM	Full-width-half-maxima
HOMO	Highest occupied molecular orbital
ITO	Indium tin oxide
IMFP	Inelastic mean free path
KPFM	Kelvin probe force microscope
LUMO	Lowest occupied molecular orbital
MEH-PPV	Poly(2-methoxy-5-(2'-ethyl-hexyloxy)-p-phenylene vinylene)
NICISS	Neutral impact collision ion scattering spectroscopy
nm	Nanometer
OPV	Organic photovoltaic
PEDOT:PSS	Poly(3,4-ethylenedioxythiophene): poly(4-styrenesulfonate)
P3HT	poly (3-hexylthiophene)
PCBM	[6,6]-phenyl-C61-butyric acid methyl ester
PPM	Parts per million
PESA	Photoelectron spectroscopy in air

Abbreviations

p-LED	Polymer light emitting diodes
PET	Polyethylene terephthalate
PLD	Pulsed laser deposition
PEN	Polyethylene naphthalate
RH	Relative humidity
RBS	Rutherford backscattering spectroscopy
SPM	Surface probe microscopy
S. E.	Secondary electron
SKPM	Scanning kelvin probe microscopy
TEM	Transmission electron microscope
TOF	Time of flight
TW	Terawatt
UV	Ultraviolet
UHV	Ultra-high vacuum
UPS	Ultraviolet photoelectron spectroscopy
VBM	Valence band maxima
XPS	X-ray photoelectron spectroscopy
ZnO	Zinc oxide